Astronomy & Astrophysics manuscript no. aa0010 March 26, 2004
(DOI: will be inserted by hand later)

MAFAGS-OS: New opacity sampling model atmospheres for A, F and G stars

I. The model and the solar flux

F. Grupp[1]

Universitäts Sternwarte München, Scheinerstr. 1, 81679 München, Germany

Received 5 January 2004 / Accepted 19 Fevruary 2004

Abstract. We present a new *opacity sampling* model atmosphere code, named MAFAGS-OS. This code, designed for stars reaching from A0 down to G9 on a solar and metal poor main sequence and up to an evolutionary stage represented by the *turnoff* is introduced in its basic input physics and modelling techniques. Fe I bound-free cross-sections of Bautista (1997) are used and convection is treated according to Canuto & Mazzitelli (1991). An $\alpha_{\rm cm}$-parameter for the efficiency of convection of 0.82 is used as determined by Bernkopf (1998) from stellar evolution requirements.
Within the process of opacity sampling, special attention is drawn to the matter of line selection. We show that a selection criterion, in which lines are chosen by their opacity weighted relative to the continuous background opacity, is useful and valid. The solar model calculated using this new code is shown to fit the measured solar flux distribution. It is also tested against the measured solar colours and leads to $U-B=0.21$ and $B-V=0.64$, in good agreement with observation. Comparison with measured centre-to-limb continuum data show only small improvement with respect to opacity-sampling type model atmospheres. This is the first of a series of 2 papers. Paper II will deal with the matter of temperature determination using Balmer lines and the infrared-flux method; furthermore it will present three *"standard"* stars analysed using this new model.

Key words. methods: numerical – Sun: infrared – Sun: photosphere – stars: atmospheres – Stars: fundamental parameters

1. Introduction

Stellar model atmospheres are among the major components for stellar analysis over the whole range of stellar temperatures and evolutionary stages.

The accuracy achieved in deriving stellar parameters, such as effective temperature $T_{\rm eff}$, gravity $\log(g)$ and Mass $\mathcal{M}$, overall metalicity [M/H] as well as micro-turbulence ξ strongly depends on the validity and accuracy of the model atmosphere on which the analysis is based. The same holds for high precision determinations of individual element abundances [X/Fe]. An accurate $T(\tau)$-law for the atmospheric structure, together with the quality of the atomic data and – of course – the quality of the observational data is responsible for the final accuracy in stellar spectroscopic and photometric analysis. Examples of the detailed influence of different atmospheric models on the spectral flux distribution and colour are investigated and presented by Castelli & Kurucz (1994) and Castelli (1999).

With this paper we present **MAFAGS-OS**, an *opacity sampling* (OS) model atmosphere program based on the *opacity distribution function* (ODF) version of the **MAFAGS** code invented by Gehren. Although unpublished as a stellar atmosphere code this model is widely used and has proven its reliability for A-, F- and G-type stars of different evolutionary stage and for various scientific questions. Some of the most recent publications based on Gehrens ODF Version of MAFAGS are: Korn et al. (2003), Mashonkina et al. (2003), Fuhrmann (2002), Gehren et al. (2001a), Gehren et al. (2001b), Mashonkina & Gehren (2001), Fuhrmann (1999), Mashonkina et al. (1999), Mashonkina et al. (1999), Fuhrmann et al. (1997), Fuhrmann et al. (1994), Fuhrmann et al. (1993) and Gehren et al. (1991).

What are the main differences between the *opacity sampling* and the *opacity distribution function* method? There is an extremely large number of known bound–bound transition (more than 20 million transitions are treated in our code) and a very large number of these absorption lines can contribute to a single point on the wavelength grid. This requires an enormous amount of calculation time and memory to calculate OS-based model atmospheres. Using modern computing facilities it becomes possible to iterate an atmosphere towards convergence within some hours of calculation time. However, calculating an extended and small-meshed grid of atmospheres for interpolation, is still out of reach for this approach. Most commonly this is circumvented by using *opacity distribution*

Send offprint requests to: F. Grupp,
e-mail: fug@usm.uni-muenchen.de

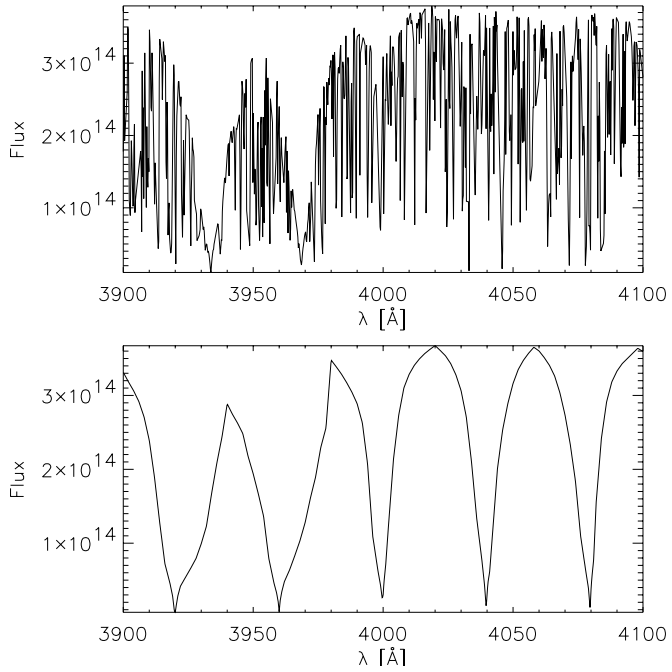

Fig. 1. Theoretical flux distribution between 3900 and 4100 Å for solar OS (*upper*) and ODF (*lower*) model.

functions. ODF are tabulated opacities on a grid of stellar atmospheric parameters such as electron pressure P_e, gas pressure P_g, temperature T and abundance mixture $[X_n/H]$ calculated for a given wavelength grid[1]. This approach allows the calculation of bound–bound opacities by interpolation on a simple 4-dimensional grid. However, as ODF-tables are only available for a few selected abundance mixtures, the individual chemical composition of stars cannot be taken into consideration properly. Furthermore the resampling and reorganisation that is done when producing ODF-tables destroys the individual spectral flux distribution in atmospheric calculations. Figure 1 shows a 200 Å band in the solar spectrum, for both ODF and OS output of our atmospheric models.

After having introduced the general assumptions and basics of our model in Sect. 2 we will turn to discuss our treatment of convective processes in Sect. 3. Section 4 deals with the sources of opacity data used in our code. Thereafter the sampling procedure and the wavelength distribution of sampling points are studied in Sect. 5. The resulting solar model is presented and compared with that of other authors in Sect. 6. Section 7 confronts the theoretical flux distributions of our models with flux measurements and solar *UBV*-colour determinations as well as with solar centre-to-limb continuum observations. A final discussion and outlook to further conclusions and applications is given in Sect. 8.

2. General assumptions for our model

Our model is based on the code of Gehren in the revised version of Reile (1987).

[1] For a brief description of ODF calculation and application see Kurucz (1979).

As shown by Fuhrmann et al. (1993) this model is almost identical to the more generally known model of Kurucz (1979).

The basic assumptions for MAFAGS are:

Coplanar 1-D model: our Model has a coplanar geometry. This simplification is well justified as the thickness of stellar atmospheres is only a small fraction of the stellar radius for the range of stellar types considered. For the Sun the atmosphere of ≈700 km thickness and <0.001 g/cm^3 density contains less than $\approx 2 \times 10^{-9}$ the solar mass. Assuming constant gravitational acceleration throughout the atmospheric layer is therefore well justified too.
Furthermore it is one-dimensional, i.e. no inhomogeneities such as granulation, sunspots, etc. are modelled. As shown by Allende Prieto et al. (2002) this will for example affect limb-darkening properties in solar type stars.

Chemical homogeneity: the stars we apply our model to have no convective mixing process that allows the processed material from the stellar core region to proceed outwards to the atmospheric layer. Due to the extreme time scales of diffusion processes (up to 10^{13} years, Kippenhahn & Weigert 1990) this kind of mixing can be neglected.

Stationarity: large-scale changes in the structure of the atmosphere are assumed to be extremely slow due to the large timescale of stellar evolution near the main sequence and near turnoff.
Convective processes are treated in a relatively new formalism, following a formulation of Canuto & Mazzitelli (1991) (henceforth CM). The influence of this new formulation in comparison to the hitherto commonly used formulation of Böhm-Vitense (1958) (BV) will be studied in detail in Sect. 3.

No chromosphere and corona: whereas the Sun and other stars have a chromosphere and corona our models transit directly, i.e. without increasing temperature towards the boundaries into space.
We have to note that individual line(-cores) may well be, and indeed are, deficient if these layers are not taken into account.

Local thermal equilibrium: local thermal equilibrium (LTE) is assumed for our atmospheres. Since we work in the regime of early A- down to late G-type stars, i.e. ≈10 000...4900 K and we do not intend to apply our models on evolved objects of extremely low $\log(g)$ this assumption should in general be justified.
Nevertheless, recent investigations show that already for the Sun we can find notable deviations from LTE. For example Zhao & Gehren (2000) find non-LTE effects in some Mg I lines corresponding to $\approx 0.05 \cdots 0.11$ dex in [Mg/Fe]. Korn et al. (2003) recently state an average non-LTE effect for Fe I lines in the Sun of ≈0.02 dex.
This kind of effect, though small for individual lines, is one of the main factors of uncertainty when calculating stellar atmospheres in the stated regime.

Flux conservation: our model uses a Feautrier-Rybicki type of temperature correction similar to the method described by Gustafsson (1971).

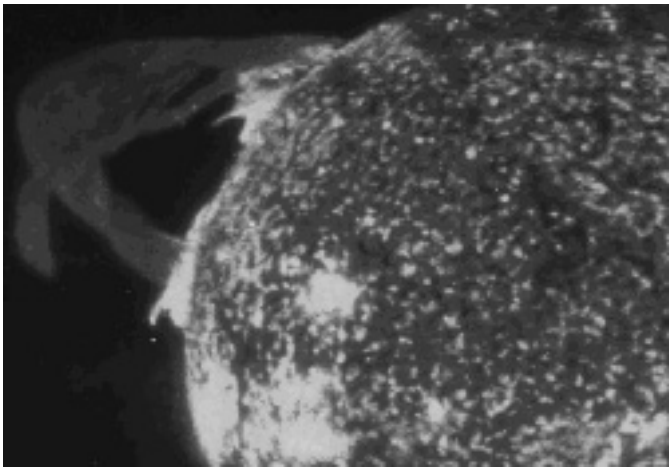

Fig. 2. The Sun: photo courtesy of the Naval Research Laboratory.

The model is iterated until flux conservation through all 80 depth points is reached on a 0.3% level for models cooler than $T_{\rm eff}$ = 8000 K and on a 0.5% level for hotter models. The total flux of the model is given by the effective temperature of the object, according to the definition:

$$F = \sigma\, T_{\rm eff}^4 \qquad (1)$$

With F the *total emergent flux* of the atmosphere.

We refer to Fig. 2 to point out that the assumptions we have presented above are indeed simplifications that have to show their validity when the model is used and its result is compared to the observations.

3. Treatment of the convective flux

We treat convection in our code according to the model proposed and described by Canuto & Mazzitelli (1991). They describe a new formalism to calculate convection that differs basically from the hitherto most commonly used treatment of convection, the so-called *mixing length theory*, which is for example represented by Böhm-Vitense (1958). The latter uses one single type of convective element with fixed geometry. This is a fairly crude simplification in view of the highly dynamic process of stellar atmospheric convection.

Canuto & Mazzitelli (1991) replace this single type of convective element by a spectrum of eddies given by a distribution function $E(k)$. For a detailed description of their method see Canuto & Mazzitelli (1991).

Following Bernkopf (1998) we use the first formulation of the mixing length Λ, which uses the known relation $\Lambda = \alpha_{\rm cm} H_p$ in which H_p the pressure scale height.

Combining MAFAGS-ODF atmospheric models with his stellar evolution code and using the stated formulation of Canuto & Mazzitelli (1991) in *both* models, Bernkopf (1998) found that with a convective efficiency $\alpha_{\rm cm} = 0.82$ he is able to fit both the Sun at its present evolutionary stage and its Balmer line spectrum . As shown by Fuhrmann et al. (1993) the Balmer line spectrum of the Sun makes it possible to determine the convective efficiency α with high accuracy. In fact Fuhrmann et al. (1993) found, within the mixing length theory of Böhm-Vitense (1958), that the agreement with the observations was best for $\alpha_{\rm bv} = 0.5$. We would like to state explicitly that a straighforward comparison of the numerical values of α in different formulations of convection is not possible by the mere numerical value.

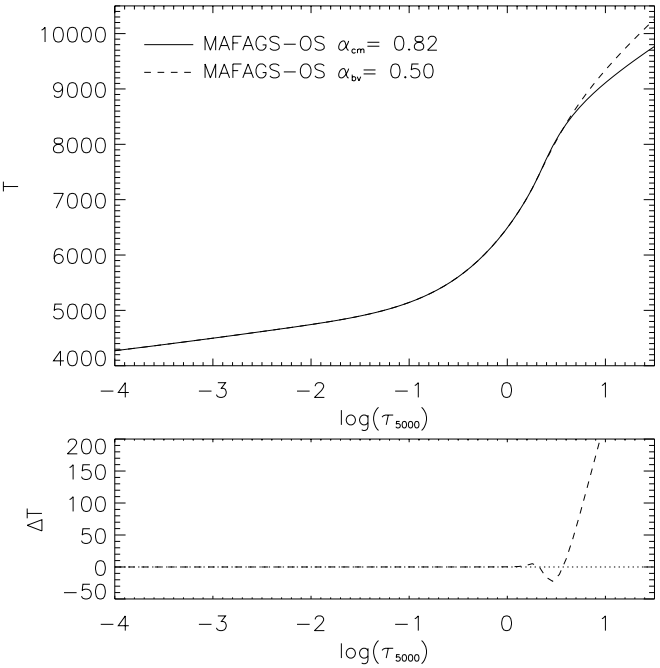

Fig. 3. Temperature structure of the MAFAGS-OS models using Böhm-Vitense theory ($\alpha_{\rm bv}$ = 0.5) and Canuto & Mazitelli theory ($\alpha_{\rm cm}$ = 0.82).

Following the approach of Bernkopf (1998) we take $\alpha_{\rm cm}$ = 0.82 as a parameter fixed by stellar evolution calculations and do not consider it as a free parameter.

Figure 3 shows a comparison of the MAFAGS-OS temperature structure for the Böhm-Vitense theory with $\alpha_{\rm bv} = 0.5$ as determined by Fuhrmann and the Canuto & Mazitelli treatment of convection using $\alpha_{\rm cm} = 0.82$ as determined by Bernkopf. The two models are almost identical outside $\log(\tau) \approx 0.1$ whereas in the inner layers the CM $\alpha_{\rm cm} = 0.82$ model is cooler, i.e. convection is less efficient. This effect can be seen more clearly in Fig. 4 which shows the percentage of flux transported by convection, together with the total and adiabatic temperature gradient for the two stated models.

4. Sources of opacity

The basic ingredients for calculating the total opacity at every distinct wavelength and depth point of our model are the sources of atomic (and molecular) data used. The better and the more complete these data are the better will the atmospheric structure be determined by our model.

It is therefore indispensable to use a very extended database of atomic data to calculate opacities within stellar atmosphere codes.

In our code we have two major sources of opacity. One comprises the so-called *continuous opacities* as they are re-

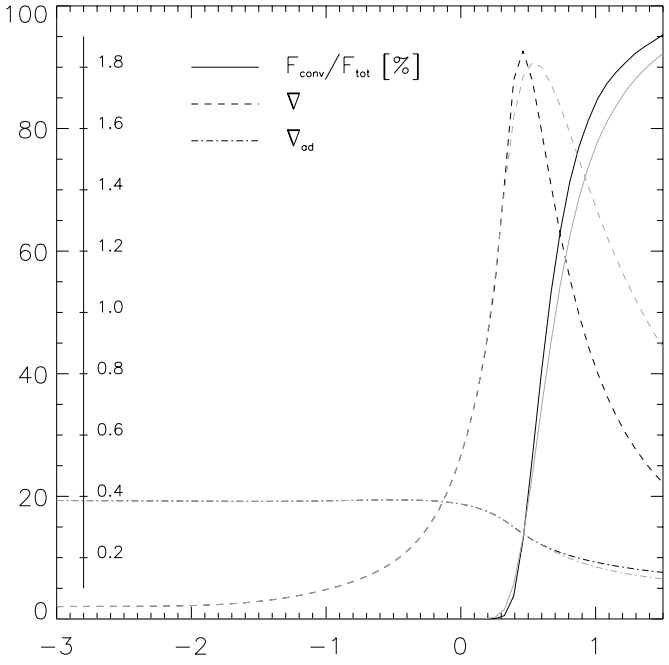

Fig. 4. Percentage of the total flux transferred by convection (full lines), total (dashed lines) and adiabatic (dot-dashed lines) temperature gradient in the MAFAGS-OS model for the two treatments of convection: Canuto & Mazitelli ($\alpha_{cm} = 0.82$) – plotted in gray, Böhm-Vitense ($\alpha_{bv} = 0.5$) – plotted in black.

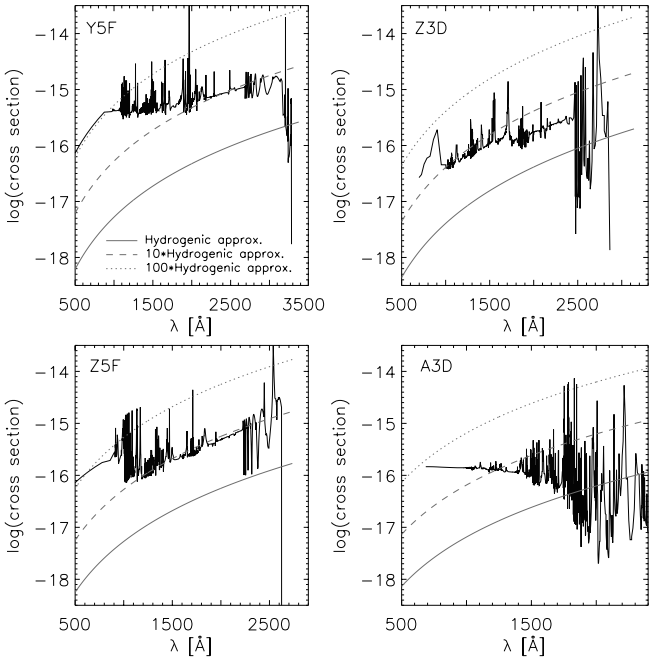

Fig. 5. Comparison between Bautista (1997) bound–free cross-sections of Fe I (full black lines) and hydrogenic approximations (full grey lines) for four individual levels of Fe I. The dashed and dotted grey lines represent 10 and 100 times the hydrogenic approximation.

lated to *bound–free* and *free–free* processes. The other source of opacity comprises *line opacities* belonging to *bound–bound* transitions in the atoms and molecules present in our atmosphere.

4.1. Continuous opacity

Free–free transitions are considered for H^- John (1988), He^- Bell et al. (1982) and H_2^- Stilley & Callaway (1970).

Absorption due to H_2 *quasi-molecules* is accounted for using Doyle (1968) and free–fee absorption cross sections for positive ions of metals are accounted for following Karzas & Latter (1961).

Rayleigh scattering is taken into account including the elements H, He and H_2.

Thompson scattering on electrons is also taken into account.

Bound–free transitions, i.e. *photoionisation* for H^- John (1988), H I and He I Kurucz (1970), H_2^+ Boggess (1959) and H_2^- Bell (1980) are considered. Neutral metals C, N, O, Mg, Al, Si, Ca and Fe are included. While we use hydrogenic approximations following Dragon & Mutschlecner (1980) for the calculations of the *bound-free* cross-sections of the elements C, N, O, Mg, Al, Si and Ca, we use the more recent calculations of Bautista (1997) to account for Fe I. Figure 5 shows the differences of simple hydrogenic approximations with the detailed calculations of Bautista (1997) for 4 selected levels. Please note that the cross sections according to Bautista are up to $10 \cdots 100$ times bigger than suggested by the hydrogenic approximation. In some resonance features they even exceed 1000 times the hydrogenic value.

While the level energies of the model atom used by Bautista (1997) are good to a few percent, which is extremely good for cross-section calculation, the wavelengths of individual features are highly insecure. It is therefore not feasible to identify these features in the crowded solar spectrum.

4.2. Line opacity

Bound–bound transitions, i.e. *absorption lines* are a crucial source of opacity for the type of stellar objects for which our model is designed.

The sources for calculating opacity data for more than 20 million lines emerging from elements of ionisation states I, II and III, and from diatomic molecules are the following:

Hydrogen lines of the Balmer series are calculated using tabulated profiles according to Vidal et al. (1973) (VCS) for H_α ... H_γ provided by Schöning & Butler (1990), the rest of the Balmer series up to H_{18} is calculated using Edmonds et al. (1967) (ESW). The exact treatment of Balmer line broadening is of minor interest for model atmosphere calculation. The line profiles calculated using ESW, VCS or the more recent calculations of Barklem et al. (2000b), Barklem et al. (2000a) and Barklem et al. (2002) differ by only a few percent. Figure 6 shows the solar temperature structure including our Balmer line treatment and switching all Balmer lines off. Even this crude 100% test shows only a difference in the temperature structure of at most 30 K. Thus, profile variations on the level of a few percent

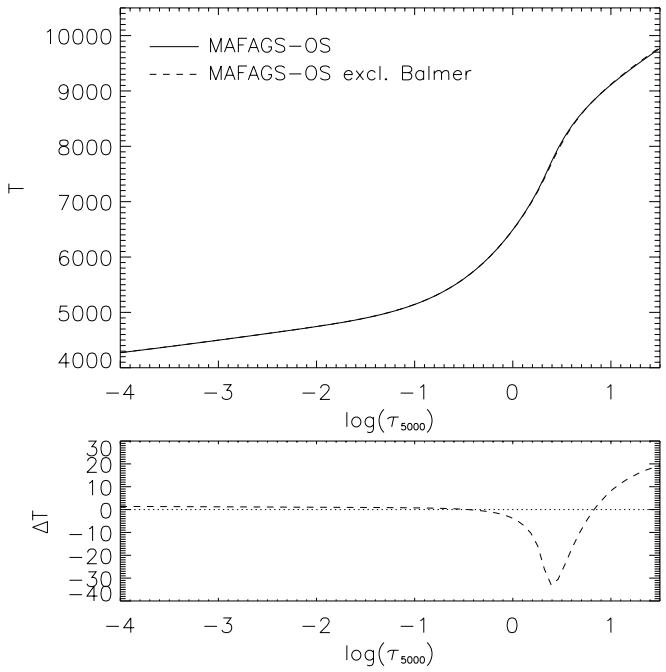

Fig. 6. MAFAGS-OS temperature structure including (full line) and excluding (dashed line) the Balmer series.

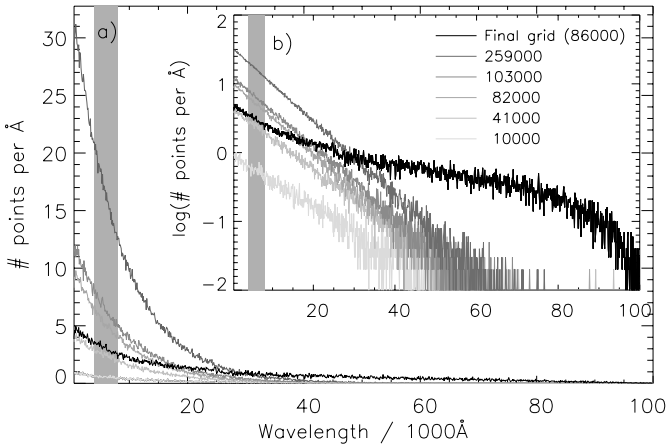

Fig. 7. Number of wavelength points per Å versus wavelength for a set of wavelength grids ranging from 10 000 up to 259 000 sampling points in λ. The final wavelength grid is plotted in black and shows an additional fraction of wavelength points in the infrared region.
b) shows the same distribution on a logarithmic scale;
Shaded in grey is the visible spectral region.

do not significantly affect the temperature structure of our solar model.

The Paschen lines P_1 ... P_{46} are calculated using VCS profiles published by Lemke (1997).

The Lyman lines L_1 ... L_{18} are calculated using the ESW theory.

Iron-group metals are taken into account based on the atomic data compilation of Kurucz (1994a), Kurucz (1994c) and Kurucz (1994b). The following broadening mechanisms are used to calculated iron-group and non-iron-group line profiles: Van der Waals broadening according to Unsöld (1955), thermal Doppler broadening, Doppler broadening due to the micro turbulent velocity ξ and the natural line width due to radiation broadening are considered.

Non-iron-group metals are accounted for using Kurucz & Bell (1995).

Diatomic molecules of the species H_2, CH, NH, OH, C_2, CN, CO, MgH, SiH and SiO are processed based on Kurucz (1993). TiO data are taken from Kurucz (1999).

The above stated sources lead to approximately 20.3 million individual absorption lines of molecules and elements in ionisation stages I, II and III for which it has to be tested if they contribute to a certain depth point of a certain wavelength point.

5. Sampling

Beside the sources of opacity data, the wavelength grid and the line-selection method are crucial for the opacity-sampling model atmosphere calculation.

Preferably one would want to have a very high number of wavelength points allowing each absorption line to be resolved by several grid points, and to use every known transition as a contributing source to each depth point at each wavelength point. Unfortunately this proceeding leads to unacceptable demands for computer time and memory.

One of the basic concepts of opacity sampling is the replacement of full resolution by a randomly chosen grid of wavelengths that represents the nature of stellar absorption lines in a statistic manner.

5.1. The wavelength grid

A suitable wavelength grid for opacity-sampling has to guarantee on the one hand that the dominant lines in photospheric spectra are resolved, and on the other hand it has to sample the wavelength range under consideration such that weak lines are accounted for in a statistical correct manner.

These requirements are extended by our knowledge of the flux distribution in stellar atmospheres. The stars we intend to model range from $T_{\rm eff} \approx 10\,000$ K (A0) down to $T_{\rm eff} \approx 5100$ K (K0). We know that there is no significant flux below $\lambda \approx 911$ Å (the Lyman edge) and that for $\lambda > 100\,000$ Å even a rough sampling will well reproduce the flux distribution in the far IR.

Figure 7 shows the distribution of sampling points for a number of grids with different density in wavelength space. The number of sampling points is selected statistically and follows a logarithmic distribution ranging from 10 000 up to 259 000 grid points . The related atmospheric structures for the solar models calculated from these grids are shown in Fig. 8. Figure 8b shows the difference of our ODF-model and the OS-models calculated based on the wavelength grids of Fig. 7. It becomes obvious from this figure that our OS-models are roughly $20 \cdots 60$ K hotter in the region of $\log(\tau) = -3 \cdots 2$ and, what is more important for the subject studied in this section, that the models differ by only a few Kelvin. This leads to the important conclusion that even a relatively small number of

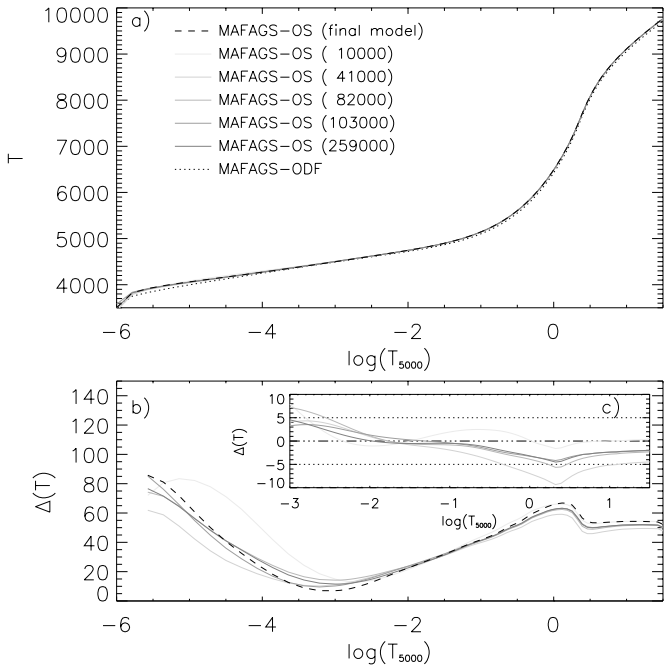

Fig. 8. Using the wavelength grids of Fig.7 the resulting atmospheric solar structures are plotted in **a)** the MAFAGS-ODF model is also plotted. **b)** Shows the difference of the OS-models with respect to our ODF-model. **c)** Plots the difference between OS-Models with different numbers of wavelength points and the finally chosen wavelength sample. The greyscales correspond to Fig. 7.

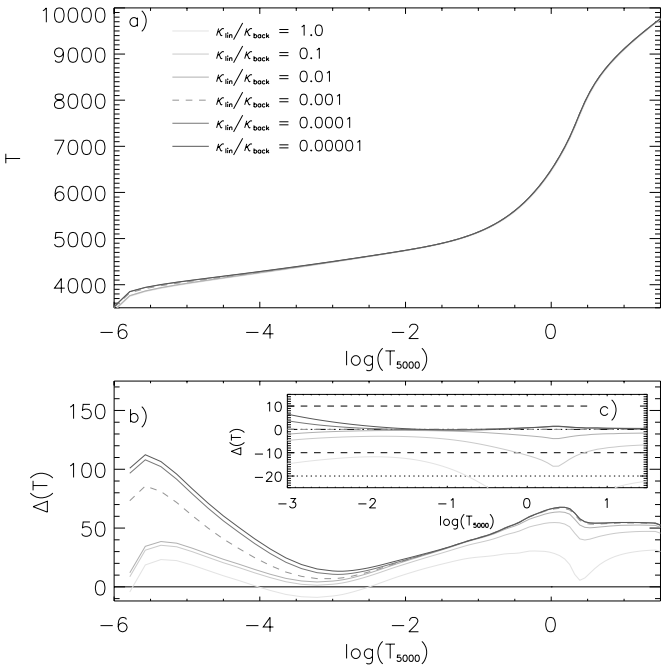

Fig. 9. Solar temperature structure for models with different ε_0 for the selection of lines considered for the model. **b)** Difference of the solar ODF-models with these OS results. **c)** The latter difference with respect to the $\varepsilon_0 = 10^{-3}$ model.

sampling points allow a statistically appropriate representation of absorption lines in the stellar atmospheres considered.

The wavelength sample chosen finally, plotted as a full black line in Figs. 7 and 8a,b has an additional number of grid points in the infrared region. Tests along the A0$\cdots$G9 main sequence considering metallicities down to [Fe/H] = −2 show that such a distribution leads to faster convergence and more stable models in the region of $\log(\tau) < -3$. The difference of the models with different numbers of sampling points following a pure logarithmic distribution and our final model is plotted in Fig. 8c. The fact, that we restrict our wavelength grid to a model of 86 000 wavelength points may lead to an uncertainty of the temperature structure within $\log(\tau) = -3 \cdots 1.5$ of up to 5 K as can be estimated from Fig. 8c.

5.2. Line selection

As it is not feasible within the given resources of computing time and memory consumption to use all 20.3 million lines of our line list as contributors to every single depth and wavelength point, a proper method of *line selection* has to be chosen.

The procedure chosen for our code was to select lines that exceed a given threshold ε_0 of opacity with respect to the background- (continuous-) opacity at at least one depth point of at least one wavelength point.

$$\varepsilon = \frac{\kappa_{\rm lin}}{\kappa_{\rm back}} \geq \varepsilon_0 \qquad (2)$$

This selection is based on the atmospheric structure achieved by iterating an ODF-model to reasonable accuracy. Afterwards each transition is tested, based on the hitherto obtained temperature structure, on the OS-wavelength-grid.

Within this procedure the selection of the threshold ε_0 is important. Together with the wavelength grid it decides – especially for weak lines – whether the lines are taken into account or not. Its value is crucial for a proper statistical treatment of the millions of weak bound–bound transitions in our sampling procedure.

Figure 9 shows the temperature structure of our sampling models for different values of ε_0 reaching from 1 down to 10^{-5} for the solar atmosphere. Figure 9b shows the difference of these models with respect to the MAFAGS-ODF model. Finally, Fig. 9c illustrates the difference between the finally chosen value of $\varepsilon_0 = 10^{-3}$ and the models with higher and lower values for ε_0.

$\varepsilon_0 = 10^{-3}$ proved to be a proper choice for A$\cdots$G stars. Once again careful selection of the value of ε_0 with respect to computing time and memory consumption leads to a source of internal errors within our atmospheres. For the most important depth range of line formation this error is of the order of ≈5 K for the range of stars covered by MAFAGS-OS.

Figures 10a,b show the final density of selected bound–bound transitions per Å. The distribution of bound–bound transitions within the elements is shown in Fig. 11, indicating the outstanding importance of iron among the other elements.

As a final interesting point we present the number of transitions having a certain *range of influence*. This *range of influence* marks the distance in Å for which a certain transition is taken into account along the wavelength grid. The number

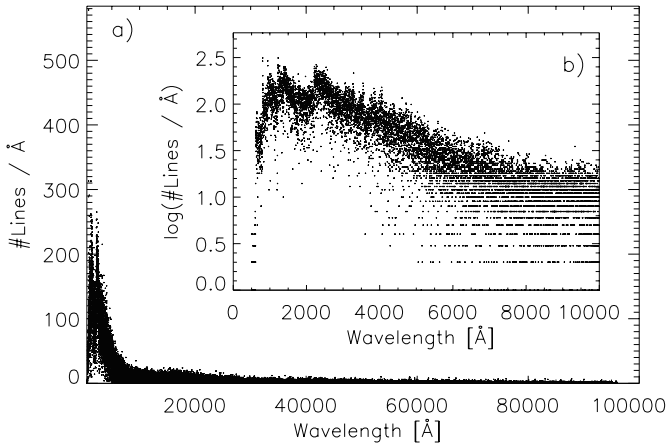

Fig. 10. Distribution of selected bound–bound transitions. Subfigure **b)** with logarithmic scale.

of lines versus this *range of influence* is plotted in Fig. 12 for both elements and diatomic molecules on a logarithmic scale. Figure 12 shows that the vast majority of bound–bound transitions needs to be taken into account only within a very small band along their central wavelength. This is even more obvious for diatomic molecules than for the elements.

6. The solar temperature structure

After having described methods and procedures for opacity calculation, we will now turn towards the resulting stellar atmospheres. This paper will be restricted to the Sun as the most prominent object to test our results for. For a trial of the new model on three further stars of different temperature and metallicity we defer the interested reader to Paper II.

To calculate the solar model the element abundances of Table 1 were applied. Note that we use the *low* iron abundance following Grevesse & Sauval (1999).

6.1. MAFAGS-OS

Table 2 presents the MAFAGS-OS solar atmosphere. The model has been calculated for the following parameters:

$$\begin{aligned} T_{\rm eff} &= 5777 \text{ K} \\ \log(g) &= 4.44 \\ [\text{Fe/H}] &= 0.00 \\ \xi &= 1.13 \text{ km/h} \end{aligned}$$

We used the 86 000-point wavelength list discussed in Sect. 5.1. and $\varepsilon_0 = 10^{-3}$ for the threshold of line selection as discussed in Sect. 5.2

6.2. Comparison with empirical models

The semi-empirical models of Holweger & Mueller (1974) and of Maltby et al. (1986) for the quiet Sun will now be compared to our model. This kind of model is determined inverting the *centre-to-limb variation* of the solar intensity, and in the case of the Holweger & Mueller (1974) model the profile of selected spectral lines.

As shown in Fig. 13, both empirical models show the same temperature structure with deviations up to 100 K. Especially in the depth range of $\log(\tau) \approx -3 \cdots 0$ the Maltby et al. (1986) model comes quite close to our OS-atmosphere, whereas inside $\log(\tau) \approx 0$ in the depth range where convection plays a major role our OS-model is significantly hotter than both empirical approaches.

Figure 14 shows the same comparison, but now we use the Böhm-Vitense (1958) mixing-length theory with $\alpha_{\rm bv} = 1.50$ to calculate our model. The differences in the model structure are smaller, but difference up to 150 K as compared with the Holweger & Mueller (1974) model and up to 100 K as compared with the Maltby et al. (1986) model remain.

These differences however are not too astonishing when keeping in mind the very different approach followed for semi-empirical and theoretical model atmospheres. Especially the deeper atmospheric regions are almost impenetrable for the method of inversion. Furthermore the three models use very different values for the solar iron abundance [Fe/H]. While Holweger & Mueller (1974) uses [Fe/H] = 7.6 and Maltby et al. (1986) uses the even higher value [Fe/H] = 7.67 we use the *low* value of Grevesse & Sauval (1999) [Fe/H] = 7.50.

6.3. Comparison with ODF-models

The most commonly used type of model atmospheres – ODF-models – will be compared to our new OS-models next. As a selection we chose the Gustafsson et al. (1975) model, the Kurucz (1979) model and our own ODF-model for comparison with OS-calculations.

Figure 15 shows these four models compared to each other. The MAFAGS-OS and MAFAGS-ODF models are calculated using CM with $\alpha_{\rm cm} = 0.82$, the Kurucz (1979) model uses BV with $\alpha_{\rm bv} = 1.50$ and Gustafsson et al. (1975) uses the mixing-length theory in the formalism of Henyey et al. (1965). It is obvious that the MAFAGS-OS model is hotter by ≈60 K at $\log(\tau) \approx -0.2$ than the MAFAGS-ODF model, with a tendency towards lower deviations in the temperature structure inside and outside this optical depth, reaching less than 15 K outside $\log(\tau) \approx -3$. Comparing with Kurucz (1979) it becomes obvious that MAFAGS-ODF and his model show a similar temperature structure outside $\log(\tau) \approx -0.5$ and differ by a larger amount in the depth range where the different treatment of convection used in these models is important. Gustafsson et al. (1975) ODF calculations together with a different formalism of calculating the convective flux lead to an atmospheric structure significantly cooler than our models inside $\log(\tau) \approx -2$.

This is why the afore mentioned comparison is repeated, calculating both MAFAGS-ODF and -OS model with the same convective treatment as used by Kurucz (1979). The results are plotted in Fig. 16. This plot verifies the results of Fuhrmann (1993) and Fuhrmann et al. (1993) wher Kurucz (1979) and MAFAGS-ODF lead to quite similar atmospheric structures. More importantly, it shows that our OS-model is indeed hotter than the comparable ODF-model by up to 60 K. Although this is not a big difference compared with the absolute temper-

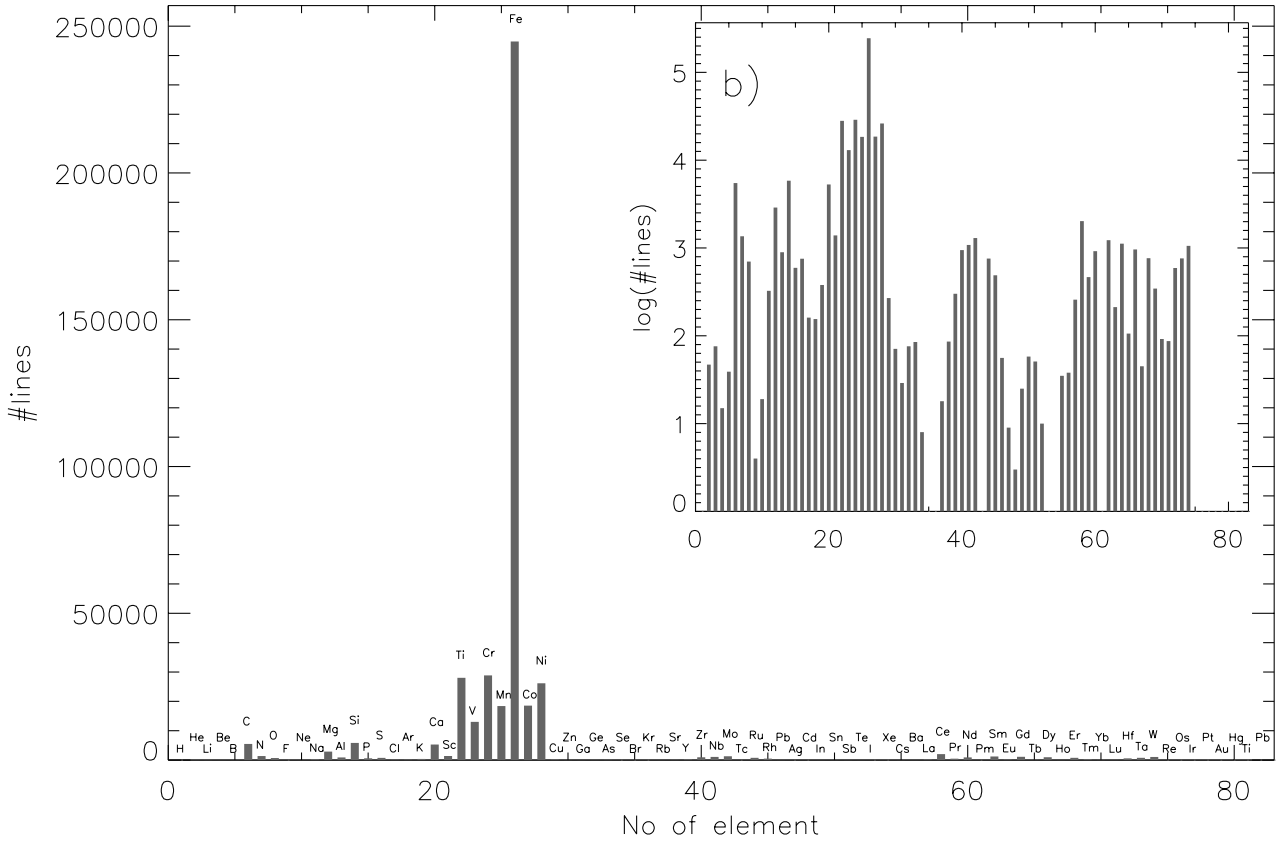

Fig. 11. Number of bound–bound transitions for all elements treated within our code.

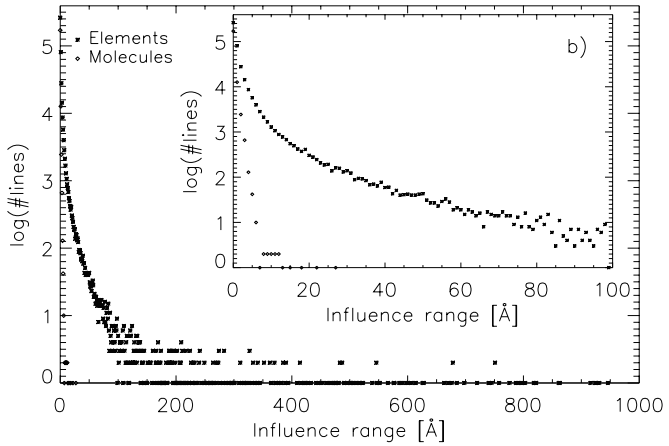

Fig. 12. Number of transitions vs. *range of influence*. Sub-figure **b)** with logarithmic scale.

ature, this should – and will – influence flux-distribution and Balmer-line temperature[2].

As a preliminary result we would like to note here that the difference between solar ODF and OS model, though not very large, extends the level where these differences can be neglected.

[2] Paper II will study the effect on Balmer-line temperature determination more extensively.

Table 1. Solar element abundance in the usual notation, i.e. $\log(N(H)) = 12$ for the 83 elements considered in our model.

Elem	Abun	Elem	Abun	Elem	Abun	Elem	Abun
H	12.00	He	11.00	Li	3.31	Be	1.42
B	2.79	C	8.55	N	7.97	O	8.87
F	4.48	Ne	8.08	Na	6.32	Mg	7.58
Al	6.49	Si	7.56	P	5.53	S	7.20
Cl	5.28	Ar	6.52	K	5.13	Ca	6.35
Sc	3.10	Ti	4.94	V	4.02	Cr	5.69
Mn	5.53	Fe	7.50	Co	4.91	Ni	6.25
Cu	4.29	Zn	4.67	Ga	3.13	Ge	3.63
As	2.37	Se	3.38	Br	2.63	Kr	3.23
Rb	2.41	Sr	2.92	Y	2.23	Zr	2.61
Nb	1.40	Mo	1.97	Ru	1.83	Rh	1.10
Pd	1.70	Ag	1.24	Cd	1.76	In	0.82
Sn	2.14	Sb	1.03	Te	2.24	I	1.51
Xe	2.23	Cs	1.13	Ba	2.22	La	1.22
Ce	1.63	Pr	0.80	Nd	1.49	Sm	0.98
Eu	0.55	Gd	1.09	Tb	0.35	Dy	1.17
Ho	0.51	Er	0.97	Tm	0.15	Yb	0.96
Lu	0.13	Hf	0.75	Ta	-0.13	W	0.69
Re	0.28	Os	1.39	Ir	1.37	Pt	1.69
Au	0.87	Hg	1.17	Ti	0.83	Pb	2.06
Bi	0.71	Th	0.09	U	-0.50		

6.4. Comparison with OS-model

As there are only few published OS-model atmospheres for the Sun we chose the one of Edvardsson et al. (1993) for

Table 2. Structure of MAFAGS-OS solar model atmosphere: Temperature [K], optical depth for λ = 5000 Å, Rosseland optical depth, gas pressure [Pa], electron pressure [Pa], Rosseland opacity.

T	τ_{5000}	$\tau_{\rm Ross}$	$P_{\rm gas}$	$P_{\rm el}$	$\kappa_{\rm Ross}$
3504	1.0E-6	4.0E-7	3.43E+1	2.13E-3	8.0E-4
3824	1.6E-6	7.2E-7	5.42E+1	4.73E-3	9.7E-4
3916	2.7E-6	1.4E-6	8.14E+1	7.30E-3	1.2E-3
3979	4.4E-6	2.6E-6	1.18E+2	1.07E-2	1.4E-3
4030	7.2E-6	4.7E-6	1.68E+2	1.51E-2	1.7E-3
4077	1.2E-5	8.4E-6	2.34E+2	2.10E-2	2.1E-3
4122	1.9E-5	1.5E-5	3.23E+2	2.88E-2	2.6E-3
4166	3.2E-5	2.6E-5	4.40E+2	3.90E-2	3.2E-3
4211	5.2E-5	4.4E-5	5.95E+2	5.25E-2	4.0E-3
4256	8.5E-5	7.6E-5	7.99E+2	7.03E-2	4.9E-3
4303	1.4E-4	1.3E-4	1.07E+3	9.37E-2	6.1E-3
4350	2.3E-4	2.2E-4	1.42E+3	1.25E-1	7.6E-3
4398	3.7E-4	3.7E-4	1.89E+3	1.65E-1	9.5E-3
4448	6.1E-4	6.1E-4	2.50E+3	2.18E-1	1.2E-2
4498	1.0E-3	1.0E-3	3.31E+3	2.89E-1	1.5E-2
4514	1.2E-3	1.2E-3	3.62E+3	3.16E-1	1.6E-2
4531	1.4E-3	1.eE-3	3.96E+3	3.45E-1	1.7E-2
4547	1.6E-3	1.7E-3	4.33E+3	3.77E-1	1.8E-2
4564	1.9E-3	2.0E-3	4.74E+3	4.13E-1	2.0E-2
4581	2.2E-3	2.4E-3	5.18E+3	4.51E-1	2.1E-2
4597	2.6E-3	2.8E-3	5.67E+3	4.93E-1	2.3E-2
4614	3.1E-3	3.3E-3	6.20E+3	5.39E-1	2.4E-2
4631	3.6E-3	3.9E-3	6.78E+3	5.89E-1	2.6E-2
4648	4.2E-3	4.6E-3	7.41E+3	6.43E-1	2.8E-2
4665	4.9E-3	5.4E-3	8.10E+3	7.03E-1	3.0E-2
4683	5.8E-3	6.3E-3	8.85E+3	7.68E-1	3.2E-2
4700	6.8E-3	7.5E-3	9.67E+3	8.34E-1	3.5E-2
4718	7.9E-3	8.8E-3	1.06E+4	9.18E-1	3.7E-2
4736	9.3E-3	1.0E-2	1.15E+4	1.00E+0	4.0E-2
4755	1.1E-2	1.2E-2	1.26E+4	1.10E+0	4.3E-2
4774	1.3E-2	1.4E-2	1.38E+4	1.20E+0	4.6E-2
4793	1.5E-2	1.7E-2	1.51E+4	1.31E+0	4.9E-2
4814	1.8E-2	2.0E-2	1.65E+4	1.44E+0	5.3E-2
4835	2.1E-2	2.4E-2	1.80E+4	1.57E+0	5.7E-2
4858	2.4E-2	2.8E-2	1.96E+4	1.72E+0	6.1E-2
4882	2.8E-2	3.3E-2	2.15E+4	1.89E+0	6.6E-2
4907	3.3E-2	3.9E-2	2.34E+4	2.08E+0	7.1E-2
4934	3.9E-2	4.5E-2	2.56E+4	2.28E+0	7.6E-2
4963	4.6E-2	5.4E-2	2.80E+4	2.51E+0	8.1E-2
4994	5.4E-2	6.3E-2	3.06E+4	2.77E+0	8.8E-2
5028	6.3E-2	7.5E-2	3.34E+4	3.07E+0	9.4E-2
5065	7.4E-2	8.8E-2	3.65E+4	3.40E+0	1.1E-1
5105	8.7E-2	1.0E-1	3.98E+4	3.77E+0	1.1E-1
5149	1.0E-1	1.2E-1	4.35E+4	4.20E+0	1.2E-1
5196	1.2E-1	1.4E-1	4.75E+4	4.70E+0	1.3E-1
5248	1.4E-1	1.7E-1	5.18E+4	5.29E+0	1.4E-1
5305	1.6E-1	2.0E-1	5.65E+4	5.98E+0	1.5E-1
5368	1.9E-1	2.4E-1	6.16E+4	6.81E+0	1.6E-1
5437	2.3E-1	2.8E-1	6.71E+4	7.83E+0	1.7E-1
5512	2.6E-1	3.3E-1	7.29E+4	9.11E+0	1.9E-1
5595	3.1E-1	3.9E-1	7.91E+4	1.08E+1	2.2E-1
5686	3.6E-1	4.6E-1	8.55E+4	1.29E+1	2.4E-1
5786	4.3E-1	5.4E-1	9.21E+4	1.58E+1	2.8E-1
5895	5.0E-1	6.4E-1	9.88E+4	1.98E+1	3.3E-1
6014	5.9E-1	7.5E-1	1.05E+5	2.53E+1	3.9E-1
6143	6.9E-1	8.9E-1	1.12E+5	3.32E+1	4.7E-1
6284	8.1E-1	1.0E+0	1.18E+5	4.43E+1	5.9E-1
6437	9.5E-1	1.2E+0	1.24E+5	6.05E+1	7.4E-1
6603	1.1E+0	1.5E+0	1.29E+5	8.41E+1	9.4E-1
6784	1.3E+0	1.7E+0	1.34E+5	1.19E+2	1.2E+0
6982	1.5E+0	2.0E+0	1.39E+5	1.71E+2	1.6E+0
7200	1.8E+0	2.4E+0	1.43E+5	2.49E+2	2.1E+0
7448	2.1E+0	2.8E+0	1.46E+5	3.74E+2	2.9E+0
7715	2.5E+0	3.3E+0	1.50E+5	5.65E+2	3.9E+0
7964	2.9E+0	4.0E+0	1.52E+5	8.10E+2	5.2E+0
8180	3.4E+0	4.7E+0	1.54E+5	1.09E+3	6.6E+0
8366	4.0E+0	5.6E+0	1.56E+5	1.40E+3	8.1E+0
8528	4.7E+0	6.7E+0	1.58E+5	1.72E+3	9.7E+0
8671	5.5E+0	7.9E+0	1.60E+5	2.05E+3	1.1E+1
8801	6.4E+0	9.4E+0	1.62E+5	2.40E+3	1.3E+1
8920	7.5E+0	1.1E+1	1.65E+5	2.76E+3	1.5E+1
9031	8.8E+0	1.3E+1	1.67E+5	3.13E+3	1.7E+1
9135	1.0E+1	1.6E+1	1.69E+5	3.53E+3	1.8E+1
9234	1.2E+1	1.9E+1	1.72E+5	3.94E+3	2.0E+1
9329	1.4E+1	2.2E+1	1.75E+5	4.38E+3	2.3E+1
9421	1.7E+1	2.6E+1	1.77E+5	4.84E+3	2.5E+1
9511	2.0E+1	3.1E+1	1.81E+5	5.33E+4	2.7E+1
9599	2.3E+1	3.7E+1	1.84E+5	5.85E+3	3.0E+1
9685	2.7E+1	4.3E+1	1.87E+5	6.41E+3	3.3E+1
9767	3.2E+1	5.1E+1	1.91E+5	6.99E+3	3.6E+1

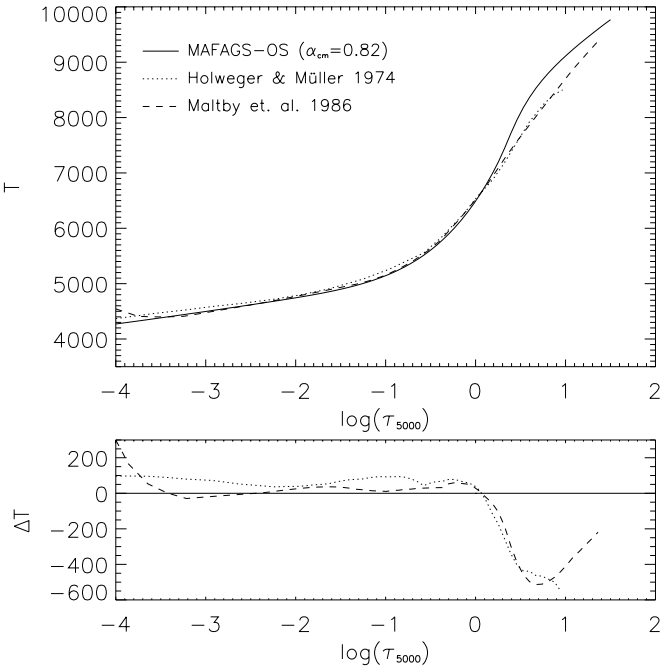

Fig. 13. Comparison between our OS-model atmosphere and the semi-empirical models of Holweger & Mueller (1974) and Maltby et al. (1986).

comparison with our approach. Edvardsson et al. (1993) use 5500 wavelength points to calculate their model. 4100 points are used calculating OS-opacities between $\lambda = 1000 \cdots 4500$ Å and another 1400 points are used for ODF-type opacity calculations in the region $\lambda > 4500$ Å.

They assume parameters that are very similar to those we use for the Sun: $T_{\rm eff}$ = 5780, $\log(g)$ = 4.44, [Fe/H] = 0.0 and ξ = 1.15 km s^{-1}, and they use the *mixing-length theory* to account for convection with α = 1.5.

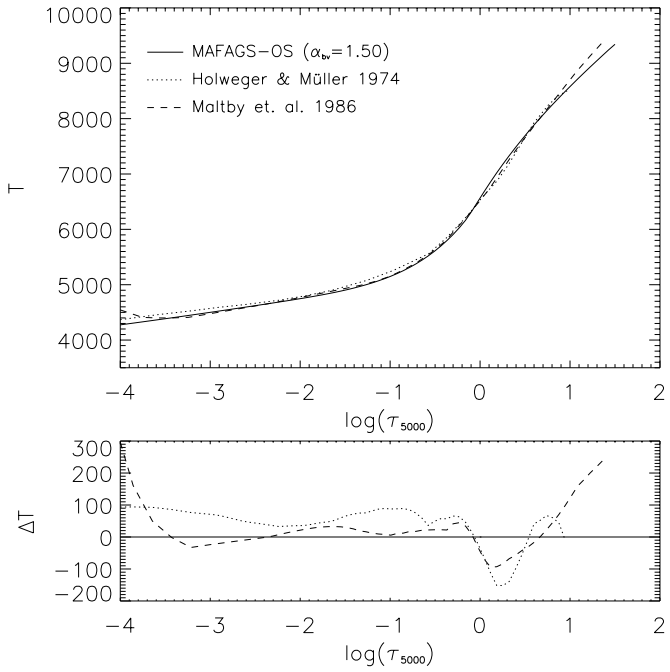

Fig. 14. Same as Fig. 13 but with a different treatment of convection for our OS-atmosphere. We use mixing-length theory with $\alpha_{\rm bv} = 1.50$ for this comparison.

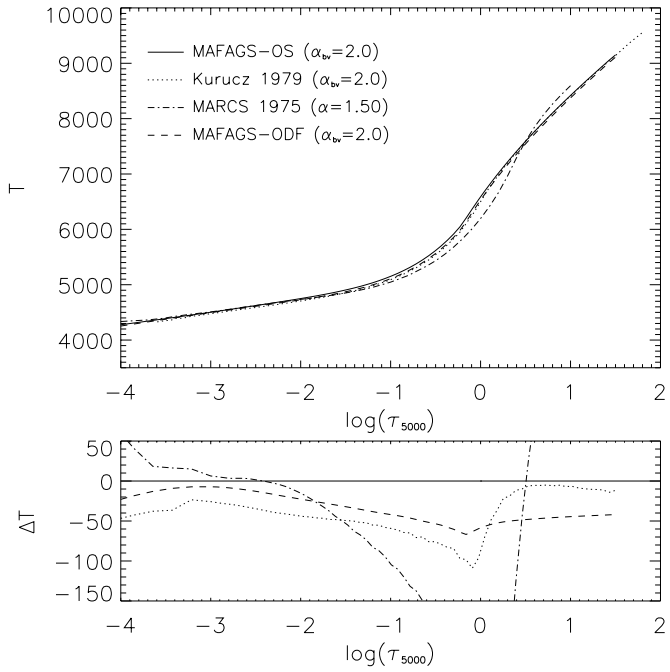

Fig. 16. Same as Fig. 15 but with a different treatment of convection for our ODF- and OS-atmosphere. We use BV theory with $\alpha_{\rm cm} = 2.0$ equal to Kurucz (1979) for this comparison.

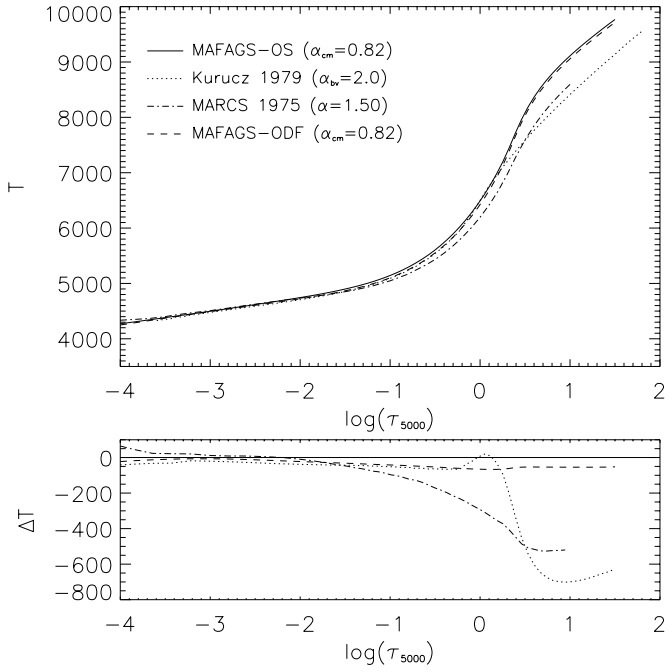

Fig. 15. Comparison of Gustafsson et al. (1975), Kurucz (1979), MAFAGS-ODF and MAFAGS-OS.

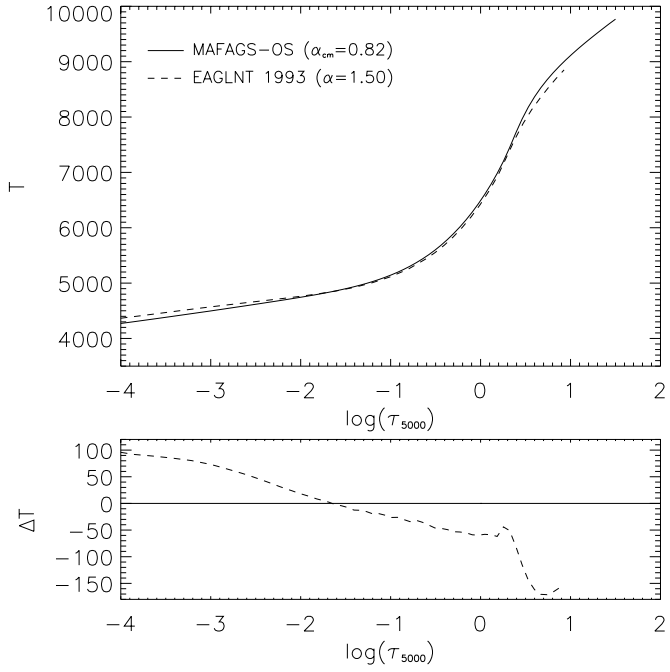

Fig. 17. Comparison between Edvardsson et al. (1993) and our own OS-model.

Figure 17 shows the result of a direct comparison between the two models. Our OS-model is cooler in the upper part of the atmosphere outside $\log(\tau) \approx -2.3$ and increasingly hotter in the deeper layers. A different treatment and efficiency of convection is also obvious in Fig. 17 inside $\log(\tau) \approx 0.3$. Turning back to Fig. 8, a low number of frequency points tends to produce higher temperatures in the range outside $\log(\tau) \approx -2.5$ and in the depth region of $\log(\tau) \approx -1.5 \cdots 0.0$. As Edvardsson et al. (1993) use only 5500 sampling points this effect may account for most of the differences at the stated depth layers.

For a more meaningful comparison of the models we calculated a MAFAGS-OS model with $\alpha_{\rm cm} = 0.65$. For this $\alpha_{\rm cm}$ the convective flux has a comparable influence in both models, although the two methods of treating convection remain clearly different. The fact that a value of $\alpha_{\rm cm}$ as used by Edvardsson et al. (1993) does not fit 1.5 does not mean anything, because

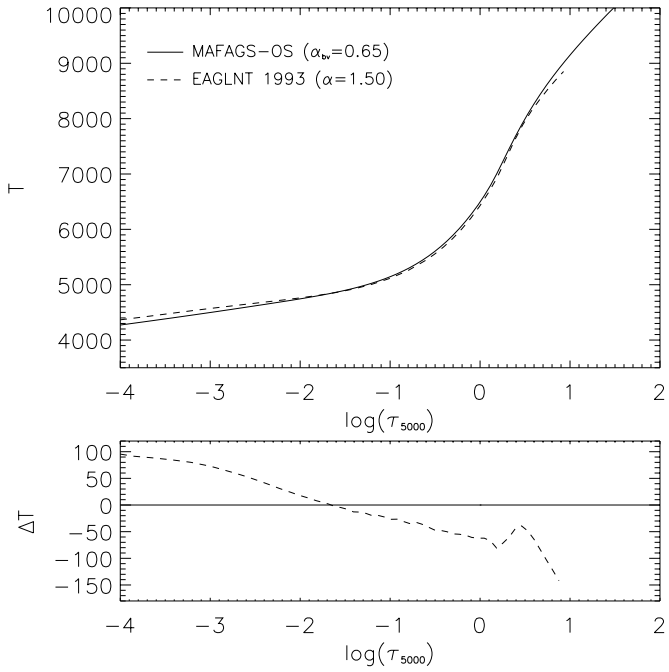

Fig. 18. Same as Fig. 17 but now with $\alpha_{\rm cm} = 0.65$ in order to compare models with compatible treatment of convection.

this value depends strongly on the exact formulation of the mixing-length theory applied[3].

The comparison of our model using $\alpha_{\rm cm} = 0.65$ with that of Edvardsson et al. (1993) is plotted in Fig. 18 and shows a continuous deviation reaching from temperatures 100 K higher than in our model at $\log(\tau) \approx -4.0$ to 150 K lower at $\log(\tau) \approx 1.0$. As Edvardsson et al. (1993) use a compatible solar iron abundance of [Fe/H] = 7.51 according to Anders & Grevesse (1989) the remaining difference can be blamed on three major differences:

- Edvardsson et al. (1993) use a much less dense wavelength grid, which according to Fig. 8 does not guarantee a well defined solar temperature structure, especially in the upper part of the atmosphere;
- they use different sources of atomic data for bound–bound transitions;
- they do not use the new radial bound–free absorption cross-sections of Bautista (1997).

7. Solar flux and colours

After having compared our model to various other approaches we will now turn back to our standard MAFAGS-OS model and compare it to solar observations. As the Sun is the only star for which we have direct access to effective temperature, mass and chemical composition[4] these tests are an important probe of the validity of our results.

[3] A discussion on this fact can be found at Bernkopf (1998).

[4] Indeed the chemical composition of the Sun is known for most elements; unfortunately there are some important elements such as C, N and O for which the abundances have not yet been determined exactly. (See for example Asplund 2003.)

7.1. Solar flux

Figure 19 shows the comparison of the theoretical flux emerging from our standard solar MAFAGS-OS model compared to the flux measurements of Neckel & Labs (1984), Houtgast (1970) and Labs & Neckel (1970). To compare measurement and model flux we used a straightforward algorithm, by folding the model theoretical flux with a Gaussian that fits the bandwidth of the filters given by flux measurements of Neckel & Labs (1984), Houtgast (1970) and Labs & Neckel (1970) for each point of their measurements. The measurements are plotted as full symbols and the corresponding model flux valuea are plotted as open diamonds in Fig. 19.

Knowing that our flux is based on the statistical method of sampling opacity data, the agreement of measured flux distribution and model prediction is remarkable. This is shown in more detail in Figs. 19b,c where the absolute and relative deviations of the model from the measurements are shown. There are remaining deficiencies around $\lambda \approx 3000$ Å, 3200 Å, 3400 Å and 3500 Å on a level reaching 20% of the flux in this region but in an overall pictureon the whole the match of measurement and theory is very close.

After the comparison with Neckel & Labs (1984), Houtgast (1970) and Labs & Neckel (1970) we turn to the more recent and higher resolved UV-data of Woods et al. (1996). Figure 20 presents the comparison of our MAFAGS-OS theoretical flux with these measurements. Again the overall agreement between measurement and theory is remarkable. The discrepancy found in Fig. 19 remains for the $\lambda \approx 3000$ Å and 3400 Å features, but vanishes for the $\lambda \approx 3200$ Å feature.

Finally we compare our theoretical flux to to the data set of Burlov-Vasiljev et al. (1995) in Fig. 21. The overall agreement is still good, but there seems to be a systematic deviation going from too much opacity in the blue to too little opacity in the red. This deviation corresponds to Figs. 10 and 11 in Burlov-Vasiljev et al. (1995) which also show this slope in the comparison of their measurements and the measurements of Neckel & Labs (1984), Shaw & Froelich (1979), Shaw (1982), Wehrli (1992), Labs et al. (1987), Lockwood et al. (1992) and Makarova et al. (1991). This figure shows, that the field of absolute solar flux measurement is not yet settled and that minor deviations can be blamed on both measurement and theoretical flux calculation. Nevertheless the overall agreement of the MAFAGS-OS theoretical model and the observation can be called good.

This good agreement of measurement and theory becomes even more obvious when we look at Fig. 22, which shows the same comparison as Fig. 19 but for the corresponding MAFAGS-ODF model. Due to the reorganisation of opacity in broad *super-lines* there is an enormous scatter in the comparison shown in Figs. 22b,c. Despite this scatter that was to be expected, there is a clear underestimation of opacity, i.e. an overestimation of the emergent flux in the whole area reaching from $\lambda \approx 2000 \cdots 4000$ Å. This reflects the problem of the so-called *missing ultraviolet opacity*. In fact the new Fe I photoionisation cross-sections of Bautista (1997) are the main reason why this problem vanishes almost completely in our MAFAGS-OS model.

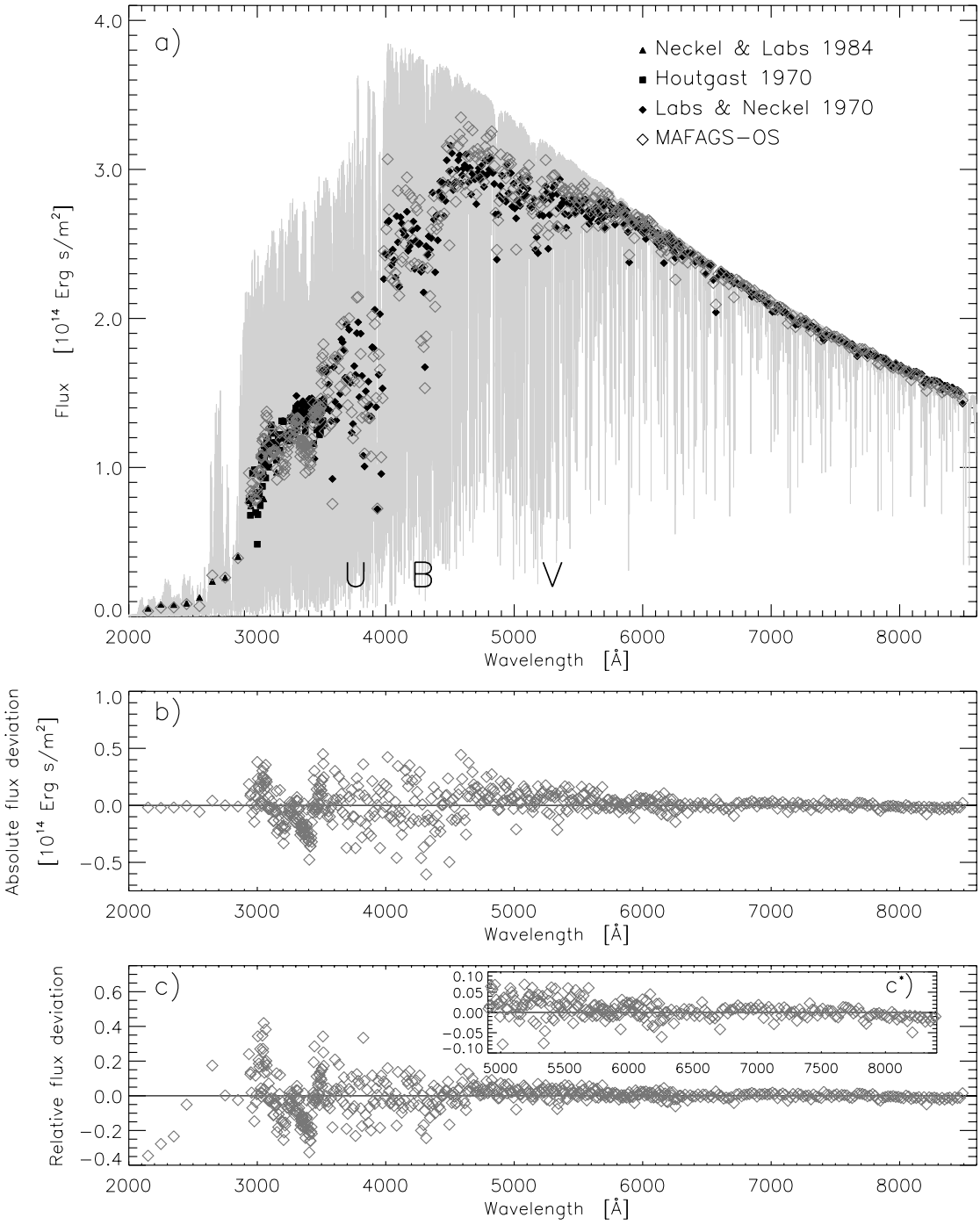

Fig. 19. Comparison between MAFAGS-OS emergent flux and the measurements of Neckel & Labs (1984), Houtgast (1970) and Labs & Neckel (1970). **a)** Total emergent flux (grey), measurements (full symbols) and model prediction (open diamonds) for the solar flux. **b)** Absolute deviation between measurement and MAFAGS-OS model prediction. **c)** Relative deviation between measurement and MAFAGS-OS model prediction. **c***) Same as **c)** but for the wavelength range $\lambda = 4800 \cdots 8800$ Å on a more detailed scale.
The central wavelengths of the Johnson *UBV* filters are indicated in **a)**.

Another obvious shortcoming of the ODF-model is the underestimation of flux in the red and infrared region. As can be seen in Fig. 22c* the flux in this region is underestimated by $3 \cdots 5\%$. Something to be worried about when using ODF-type models for *infrared-flux-method* temperature determination. This will be studied in further detail in Paper II.

For a final picture of our flux studies we present a direct comparison between MAFAGS-OS and MAFAGS-ODF emergent flux in Fig. 23.

Recovering some missing UV-opacity together with the requirement of flux conservation leads to a reorganisation of the emergent flux. This redistribution of flux from the UV to the red

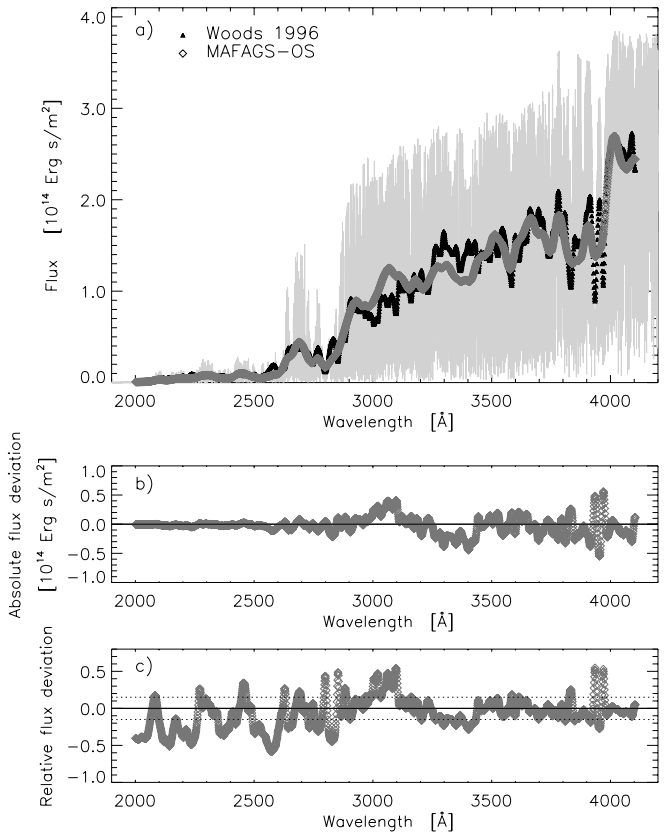

Fig. 20. Same as Fig. 19**a)–c)** but showing the comparison of MAFAGS-OS and Woods et al. (1996). The dotted line in **c)** corresponds to a 15% error as stated by the authors for their measurements.

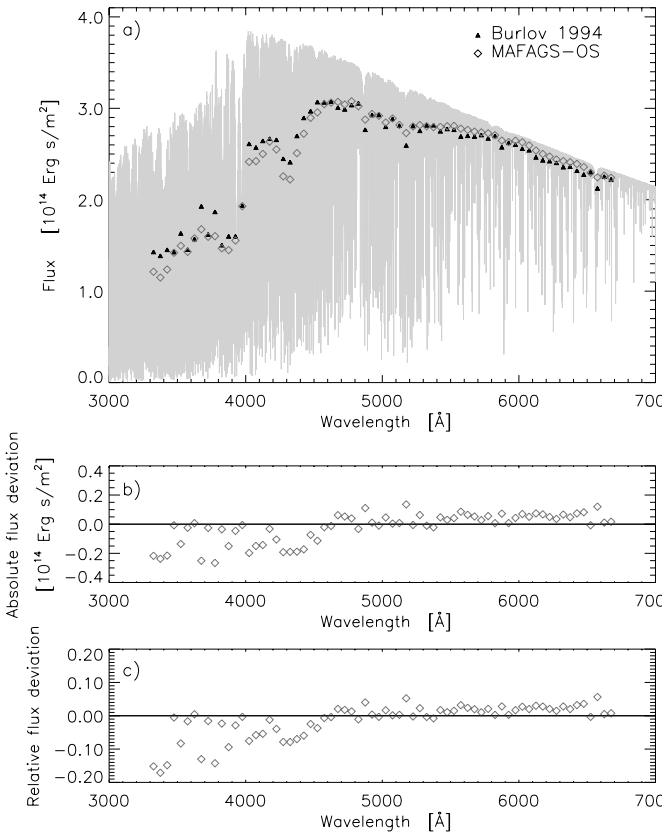

Fig. 21. Same as Figs. 19**a)–c)** but showing the comparison of MAFAGS-OS and Burlov-Vasiljev et al. (1995).

becomes obvious in Figs. 23b,c. As stated above, this redistribution needs to be investigated when discussing the *infrared-flux-method* temperature determination in Paper II.

7.2. UBV-colours of the Sun

The remarkably good agreement in the overall flux distribution encourages us to investigate the Johnson-*UBV* solar colours as well.

Table 3 shows theoretical colour determinations for the Buser & Kurucz (1992) model ATLAS9 (B&K 93), MAFAGS-ODF (ODF), MAFAGS-OS (OS) using the standard 86 000 wavelengths list and MAFAGS-OS (OS big) using our most dense 259 000 wavelength sampling list. We use the filter definitions of Buser (1978) to compute theoretical colours from our models emergent flux. The zero points, $U - B = 0$ and $B-V = 0$ are fitted to the corresponding model type Vega atmosphere. Vegas stellar parameters were chosen following Castelli & Kurucz (1994): $T_{\rm eff} = 9550$ K, $\log(g) = 3.95$, [M/H] $= -0.5$ and $\xi = 2.0$ km s^{-1}.

First of all we would like to outline the remarkable agreement between Buser & Kurucz (1992) and our own ODF model. Based on the same set of ODF-data, ATLAS and MAFAGS produce similar results as shown by Fuhrmann et al. (1993) for the temperature structure of both models.

Another important fact is the difference between MAFAGS-OS models with different numbers of wavelength points. Although the two models have a very similar temperature structure they lead to different values for the $U - B$ colour index. This shows that the number of wavelength points in the standard model is dense enough for temperature structure calculation, but it might not be dense enough for colour integration. This has to be remembered for OS-model theoretical colour indices work.

Table 3. Theoretical colours of the Sun for the ATLAS9 ODF model according to Buser & Kurucz (1992), for MAFAGS-ODF, MAFAGS-OS with standard wavelength list (86 000 points) and MAFAGS-OS with our maximum wavelength list (259 000 points).

Colour	B&K 92	ODF	OS	OS big
$U - B$	0.08	0.08	0.21	0.19
$B - V$	0.59	0.59	0.64	0.64

Table 4. Solar colour observations.

Colour	Observation	Source
$U - B$	0.195	Neckel (1994)
	0.183 ± 0.020	Tüg & Schmidt-Kaler (1982)
$B - V$	0.686 ± 0.011	Tüg & Schmidt-Kaler (1982)
	0.68 ± 0.005	Gray (1995)
	0.65	Neckel (1994)
	0.642 ± 0.004	Cayrel de Strobel (1996)
	0.62	Makarova et al. (1989)

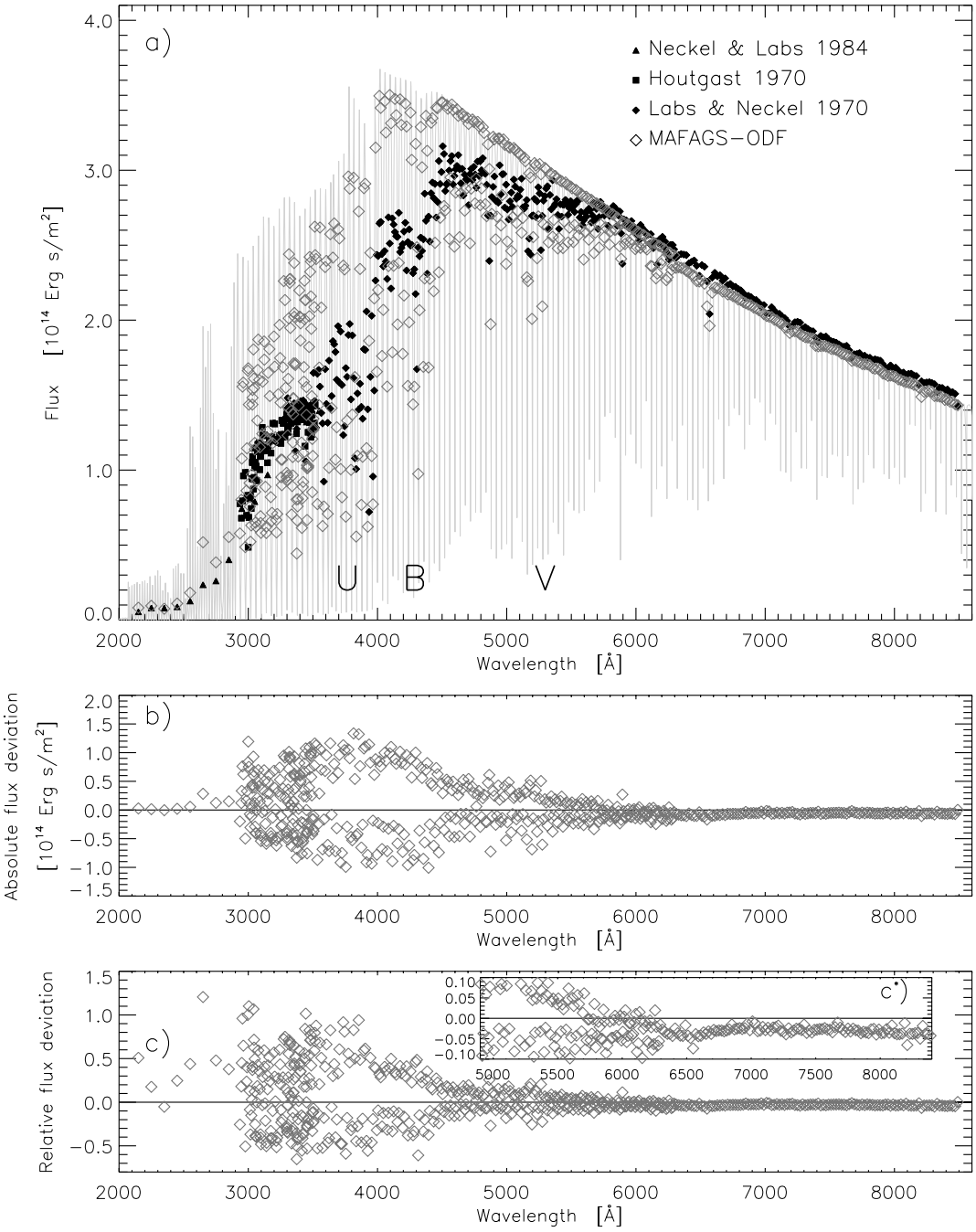

Fig. 22. Same as Fig. 19 but for the MAFAGS-ODF solar model.

Comparing the theoretical colours of Table 3 with the colour measurements of Table 4 it can be seen that both $U-B$ and $B-V$ are far better reproduced by MAFAGS-OS than by the ODF-type-models. Furthermore we find a better agreement between the $U-B$ index of the sampling model with the more dense wavelength grid and the observed values.

7.3. Centre-to-limb variation of the solar continuum

As a last test we will now turn to studying the solar centre-to-limb variation. We compare our theoretical results with the the measurements of Pierce & Slaughter (1977) and Pierce et al. (1977) and their fifth order polynomial fits in $\mu = \cos(\theta)$ of the fraction $I(\lambda,\mu)/I(\lambda,1.0)$. In a direct approach we choose the angular sampling points of MAFAGS for comparison, i.e. $\mu = 0.93$, $\mu = 0.67$, $\mu = 0.33$ and $\mu = 0.07$. Figure 24 compares our theoretical MAFAGS-OS data to the measurements. The overall fit cannot be called satisfactory. Although the difference between MAFAGS-ODF model and measurement, shown in Fig. 25 decreases slightly in the regions below $\lambda = 7000$ Å and above $\lambda = 18\,000$ Å the deviations between the MAFAGS-OS theoretical model and the measurement still

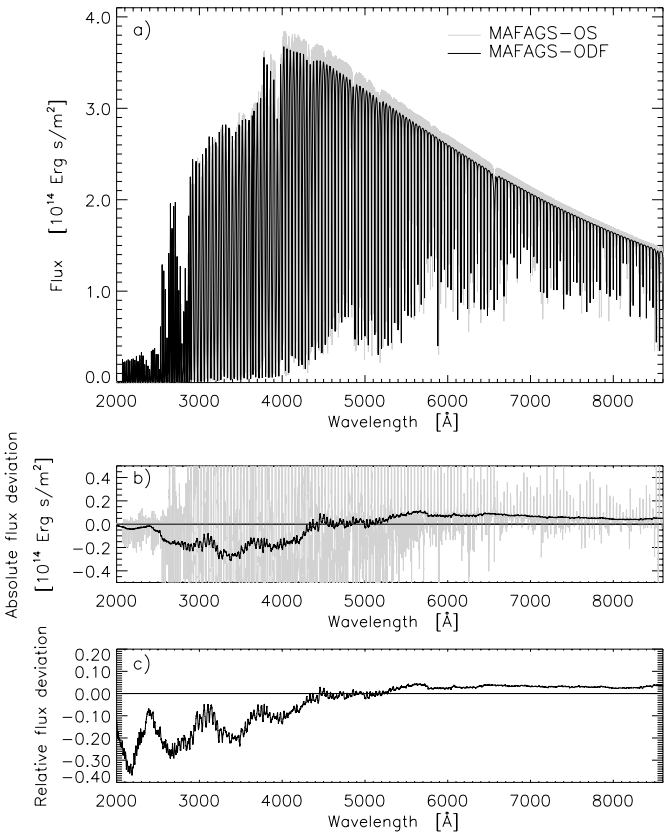

Fig. 23. a) Direct comparison of MAFAGS-OS (grey) and MAFAGS-ODF (black) flux. **b)** Absolute deviation of MAFAGS-OS and MAFAGS-ODF (grey) and deviation of the approximate continuum level (black). **c)** Relative deviation of the approximate continuum.

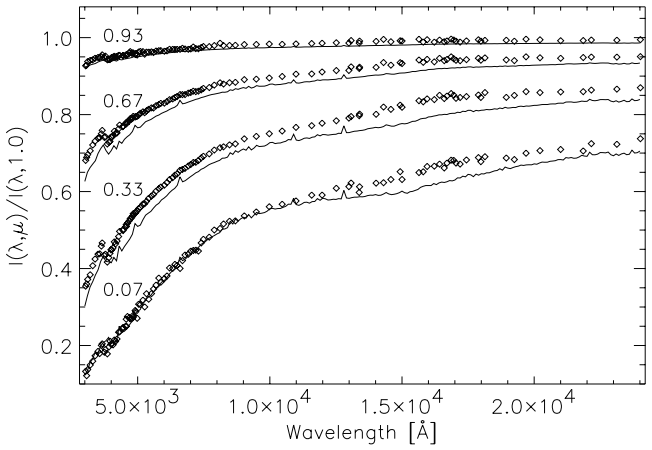

Fig. 24. Comparison of the MAFAGS-OS (full line) model intensity fraction $I(\lambda,\mu)/I(\lambda,1.0)$ and measurements (open diamonds) ofPierce & Slaughter (1977) and Pierce et al. (1977). From top to bottom: μ = 0.93, μ = 0.67, μ = 0.33 and μ = 0.07.

remain. This becomes even more obvious when comparing Figs. 24 to 26 showing the Holweger & Mueller (1974) solar model intensities. In fact one of the major inputs when inverting solar measurements to atmospheric structure in Holweger & Mueller (1974) is the centre-to-limb variation displayed in Fig. 26, and it is therefore no surprise that measurement and theory fit each other for this model.

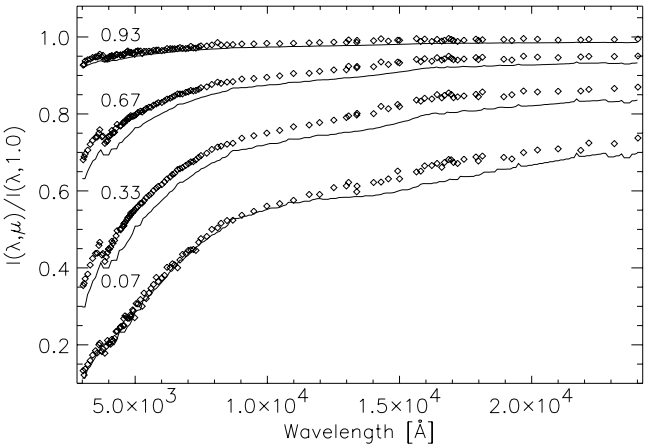

Fig. 25. Same as Fig. 24 but showing the MAFAGS-ODF model.

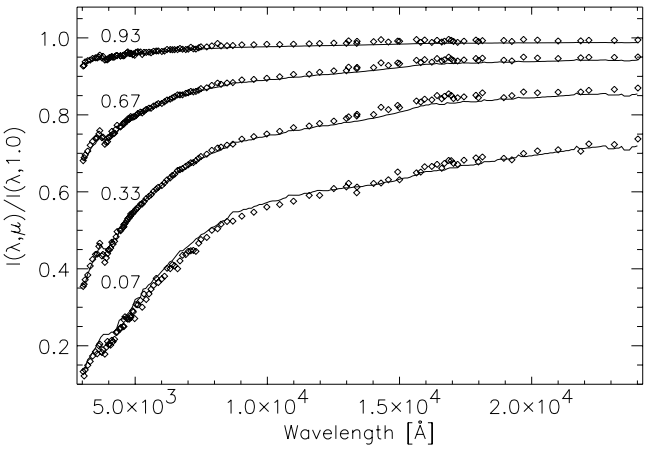

Fig. 26. Same as Fig. 24 but showing the Holweger & Mueller (1974) model.

The deviations found for MAFAGS-OS in Fig. 24 resemble the results of Blackwell et al. (1995). Their Fig. 11 shows similar results for the NMARCS model atmosphere code.

8. Discussion

The new *opacity sampling* version of the stellar atmosphere calculation code MAFAGS is introduced in this paper.

MAFAGS-OS uses a very large database of line data and recent calculations of Fe I bound-free cross sections. Extensive testing was done searching for a proper wavelength distribution and density for sampling and choosing a proper criterion for bound–bound line selection. These tests were carried out along the solar metallicity and metal poor main sequence reaching from A0 down to G9 stars and for the corresponding objects at their turnoff evolutionary stage.

Although it still shows some remaining deficiencies, the model reproduces the measured solar flux distribution to a high level of accordance. Most notably it shows much better agreement than the corresponding ODF model does. The same holds for solar colours. $U-B$ and $B-V$ colour indices are well reproduced by the OS-model, deficiencies shown by the ODF models are absent.

Table 5. Internal errors of the model.

Source	Value
Wavelength sampling list	±5 K
Line selection	±5 K
Flux conservation (0.3%)	±5 K
Overall	±10 K

Concerning the continuum centre-to-limb variation of the Sun, the discrepancies shown by ODF-type models are somewhat lessened but still remain at an unsatisfactory leve. Whereas the solar model of Holweger & Mueller (1974) that is designed to fit the centre-to-limb variation fails to conserve flux throughout the atmosphere, our theoretical models based on the principle of flux conservation fail to reproduce solar center-to-limb measurements. This can be taken to indicate the limitations of 1D theoretical modeling of stellar atmospheres.

On the whole, the new model increases the agreement with observation although the changes in the atmospheric structure, which tends to be $40\cdots60$ K hotter than it is in MAFAGS-ODF, are relatively small. While the model produces higher UV opacities and reduces the so-called *missing opacity* problem, there is an obvious shift of flux towards the IR. The solar infrared flux is therefore increased by ≈4% with respect to the ODF model, producing a better fit to the measured data. Both the increased IR flux and the changed temperature structure will affect popular methods of stellar effective temperature determination. The IR-flux method and Balmer-line temperature will need to be revisited. This is in fact a central item of Paper II.

8.1. Internal errors of the model

Quantitative error analysis in theoretical model atmospheres is hardly amenable to investigation. This is because for central input data, such as opacities, it is almost impossible to estimate accuracy or error ranges.

Nevertheless we will try and give an idea of those *internal* errors that can be estimated in Table 5. In this list we return to the errors estimated for the wavelength sampling list (Sect. 5.1) and line selection (Sect. 5.2). Another internal source of error can be blamed on a finite value of deviation from flux conservation. We accept a deviation from flux conservation at a 0.3% level for the final iteration of our model, leading to an uncertainty in temperature structure of ≈5 K. All other sources of uncertainty introduced by atomic data cannot be called *internal* sources of errors and it is unfortunately almost impossible to estimate any errors within this data.

For the internal errors, assuming that they are uncorrelated we get a total error of ≈ ± 10 K.

8.2. Outlook

Allowing a free mixture of element abundances in the stellar atmosphere opacity-sampling models will be extremely useful for stellar objects with atmospheric compositions that differ significantly from the (scaled) solar one. This holds true for metal poor stars showing significant α-element enhancement and for chemically peculiar stars such as Ap-Stars.

Paper II will deal with a sample of stars of different spectral type and evolutionary stage in order to prove that it is reasonable to use MAFAGS-OSMAFAGS-OS over a wide range of stellar objects.

The influence of the changed temperature structure and increased infrared flux on two methods of effective temperature determination, infrared-flux method and Balmer-line temperatures will be studied in detail.

MAFAGS-OS atmospheric models can be calculated on demand for interested readers. Please contact the author via E-mail.

Acknowledgements. Thanks goes to Thomas Gehren, Klaus Fuhrmann and Jan Bernkopf for their continuous work in improving MAFAGS and for many helpful hints and discussions. Thank you Constance for the data input.
This is also the place to say thanks to Jens Blanck and Michael Dörfle from SIEMENS Munich. By giving me the opportunity to work on a 20 h a week job they made it possible to continue my scientific work. Unfortunately this job has become abolished by decision of SIEMENS upper management.

References

Allende, Prieto, C., Lambert, D. L., & Asplund, M. 2002, ApJ, 573, L137
Anders, E., & Grevesse, N. 1989, Geochim. Cosmochim. Acta, 53, 197
Asplund, M. 2003, in ASP Conf. Ser., 301
Böhm-Vitense, E. 1958, Zeitschrift Astrophysics, 46, 108
Barklem, P. S., Piskunov, N., & O'Mara, B. J. 2000a, A&A, 363, 1091
Barklem, P. S., Piskunov, N., & O'Mara, B. J. 2000b, A&A, 355, L5
Barklem, P. S., Stempels, H. C., Allende Prieto, C., et al. 2002, A&A, 385, 951
Bautista, M. A. 1997, A&AS, 122, 167
Bell, K. 1980, J. Phys B, 13, 1859
Bell, K., Berrington, K., & Croskery, J. 1982, J. Phys B, 15, 977
Bernkopf, J. 1998, A&A, 332, 127
Blackwell, D. E., Lynas-Gray, A. E., & Smith, G. 1995, A&A, 296, 217
Boggess, A. I. 1959, ApJ, 129, 432
Burlov-Vasiljev, K. A., Gurtovenko, E. A., & Matvejev, Y. B. 1995, Sol. Phys., 157, 51
Buser, R. 1978, A&A, 62, 411
Buser, R., & Kurucz, R. L. 1992, A&A, 264, 557
Canuto, V. M., & Mazzitelli, I. 1991, ApJ, 370, 295
Castelli, F. 1999, A&A, 346, 564
Castelli, F., & Kurucz, R. L. 1994, A&A, 281, 817
Cayrel de Strobel, G. 1996, A&AR, 7, 243
Doyle, R. O. 1968, ApJ, 153, 987
Dragon, J. N., & Mutschlecner, J. P. 1980, ApJ, 239, 1045
Edmonds, F., Schlüter, H., & Wells, D. 1967, Mem. R.A.S, 271
Edvardsson, B., Andersen, J., Gustafsson, B., et al. 1993, A&A, 275, 101
Fuhrmann, K. 1993, Ph.D. Thesis, Universitäts Sternwarte München
Fuhrmann, K. 1999, Ap&SS, 265, 265
Fuhrmann, K. 2002, New Astron., 7, 161
Fuhrmann, K., Axer, M., & Gehren, T. 1993, A&A, 271, 451
Fuhrmann, K., Axer, M., & Gehren, T. 1994, A&A, 285, 585

Fuhrmann, K., Pfeiffer, M., Frank, C., Reetz, J., & Gehren, T. 1997, A&A, 323, 909
Gehren, T., Butler, K., Mashonkina, L., Reetz, J., & Shi, J. 2001a, A&A, 366, 981
Gehren, T., Korn, A. J., & Shi, J. 2001b, A&A, 380, 645
Gehren, T., Reile, C., & Steenbock, W. 1991, in Stellar Atmospheres - Beyond Classical Models, NATO ASIC Proc., 341, 387
Gray, D. F. 1995, PASP, 107, 120
Grevesse, N., & Sauval, A. J. 1999, A&A, 347, 348
Gustafsson, B. 1971, A&A, 10, 187
Gustafsson, B., Bell, R. A., Eriksson, K., & Nordlund, A. 1975, A&A, 42, 407
Henyey, L., Vardya, M. S., & Bodenheimer, P. 1965, ApJ, 142, 841
Holweger, H., & Mueller, E. A. 1974, Sol. Phys., 39, 19
Houtgast, J. 1970, Sol. Phys., 15, 273
John, T. L. 1988, A&A, 193, 189
Karzas, W. J., & Latter, R. 1961, ApJS, 6, 167
Kippenhahn, R., & Weigert, A. 1990, Stellar Structure and Evolution, ed. A. Library (Springer Verlag)
Korn, A. J., Shi, J., & Gehren, T. 2003, A&A, 407, 691
Kurucz, R. 1993, Diatomic Molecular Data for Opacity Calculations, Kurucz CD-ROM No. 15, Cambridge, Mass.: Smithsonian Astrophysical Observatory, 15
Kurucz, R. 1994a, Atomic Data for Ca, Sc, Ti, V, and Cr. Kurucz CD-ROM No. 20, Cambridge, Mass.: Smithsonian Astrophysical Observatory, 20
Kurucz, R. 1994b, Atomic Data for Fe and Ni, Kurucz CD-ROM No. 22, Cambridge, Mass.: Smithsonian Astrophysical Observatory, 22
Kurucz, R. 1994c, Atomic Data for Mn and Co, Kurucz CD-ROM No. 21, Cambridge, Mass.: Smithsonian Astrophysical Observatory, 21
Kurucz, R. 1999, 1999 TiO linelist from Schwenke (1998). Kurucz CD-ROM No. 24, Cambridge, Mass.: Smithsonian Astrophysical Observatory, 24
Kurucz, R., & Bell, B. 1995, Atomic Line Data, Kurucz CD-ROM No. 23, Cambridge, Mass.: Smithsonian Astrophysical Observatory, 23
Kurucz, R. L. 1970, SAO Special Report, 309
Kurucz, R. L. 1979, ApJS, 40, 1
Labs, D., & Neckel, H. 1970, Sol. Phys., 15, 79
Labs, D., Neckel, H., Simon, P. C., & Thuillier, G. 1987, Sol. Phys., 107, 203
Lemke, M. 1997, A&AS, 122, 285
Lockwood, G. W., Tueg, H., & White, N. M. 1992, ApJ, 390, 668
Makarova, E. A., Kharitonov, A. V., & Kazachevskaia, T. V. 1991, Potok solnechnogo izlucheniia (Moskva : Nauka), Glav. red. fiziko-matematicheskoi lit-ry
Makarova, E. A., Knyyazeva, L. N., & Kharitonov, A. V. 1989, AZh, 66, 583
Maltby, P., Avrett, E. H., Carlsson, M., et al. 1986, ApJ, 306, 284
Mashonkina, L., & Gehren, T. 2001, A&A, 376, 232
Mashonkina, L., Gehren, T., & Bikmaev, I. 1999, A&A, 343, 519
Mashonkina, L., Gehren, T., Travaglio, C., & Borkova, T. 2003, A&A, 397, 275
Neckel, H. 1994, in IAU Coll., 143
Neckel, H., & Labs, D. 1984, Sol. Phys., 90, 205
Pierce, A. K., & Slaughter, C. D. 1977, Sol. Phys., 51, 25
Pierce, A. K., Slaughter, C. D., & Weinberger, D. 1977, Sol. Phys., 52, 179
Reile, C. 1987, Diplomarbeit, Universitäts Sternwarte München
Schöning, T., & Butler, K. 1990, Private communications
Shaw, G. E. 1982, Appl. Opt., 21, 2006
Shaw, G. E., & Froelich, C. 1979, in Solar-Terrestrial Influences on Weather and Climate, 69
Stilley, J. L., & Callaway, J. 1970, ApJ, 160, 245
Tüg, H., & Schmidt-Kaler, T. 1982, Mitteilungen der Astronomischen Gesellschaft Hamburg, 55, 18
Unsöld, A. 1955, Physik der Sternatmospharen, MIT besonderer Berucksichtigung der Sonne (Berlin: Springer)
Vidal, C., Cooper, J., & Smith, E. 1973, ApJS, 37
Wehrli, C. 1992, in Solar Electromagnetic Radiation Study for Solar Cycle 22, 54
Woods, T. N., Prinz, D. K., Rottman, G. J., et al. 1996, J. Geophys. Res., 101, 9541
Zhao, G., & Gehren, T. 2000, A&A, 362, 1077